A novel noncontact detection method of surgeon's operation for a master-slave endovascular surgery robot

Yan Zhao, Huiming Xing, Shuxiang Guo, Yuxin Wang, Jinxin Cui, Youchun Ma, Yu Liu, Xinke Liu, Junqiang Feng & Youxiang Li

Medical & Biological Engineering & Computing

ISSN 0140-0118

Med Biol Eng Comput
DOI 10.1007/s11517-020-02143-7

Springer

Medical & Biological Engineering & Computing
https://doi.org/10.1007/s11517-020-02143-7

ORIGINAL ARTICLE

A novel noncontact detection method of surgeon's operation for a master-slave endovascular surgery robot

Yan Zhao[1,2] · Huiming Xing[2] · Shuxiang Guo[2,3] · Yuxin Wang[2] · Jinxin Cui[2] · Youchun Ma[2] · Yu Liu[2] · Xinke Liu[4,5] · Junqiang Feng[4] · Youxiang Li[4]

Received: 20 June 2019 / Accepted: 11 February 2020

Abstract

Master-slave endovascular interventional surgery (EIS) robots have brought revolutionary advantages to traditional EIS, such as avoiding X-ray radiation to the surgeon and improving surgical precision and safety. However, the master controllers of most of the current EIS robots always lead to bad human-machine interaction, because of the difference in nature between the rigid operating handle and the flexible medical catheter used in EIS. In this paper, a noncontact detection method is proposed, and a novel master controller is developed to realize real-time detection of surgeon's operation without interference to the surgeon. A medical catheter is used as the operating handle. It is enabled by using FAST corner detection algorithm and optical flow algorithm to track the corner points of the continuous markers on a designed sensing pipe. A mathematical model is established to calculate the axial and rotational motion of the sensing pipe according to the moving distance of the corner points in image coordinates. A master-slave EIS robot system is constructed by integrating the proposed master controller and a developed slave robot. Surgical task performance evaluation in an endovascular evaluator (EVE) is conducted, and the results indicate that the proposed detection method breaks through the axial measuring range limitation of the previous marker-based detection method. In addition, the rotational detection error is reduced by 92.5% compared with the previous laser-based detection method. The results also demonstrate the capability and efficiency of the proposed master controller to control the slave robot for surgical task implementation.

Keywords Endovascular surgery robot · Master controller · Surgeon's operation detection · Continuous noncontact detection

Yan Zhao and Huiming Xing contributed equally to this work.

✉ Shuxiang Guo
guoshuxiang@bit.edu.cn

[1] School of Mechanical Engineering, Hebei University of Technology, No.5340 Rd. Xiping, Beichen District, Tianjin 300401, China

[2] Key Laboratory of Convergence Biomedical Engineering System and Healthcare Technology, The Ministry of Industry and Information Technology, School of Life Science, Beijing Institute of Technology, No.5, Zhongguancun South Street, Haidian District, Beijing 100081, China

[3] Faculty of Engineering, Kagawa University, 2217-20 Hayashi-cho, Takamatsu, Kagawa 760-8521, Japan

[4] Department of Interventional Neuroradiology, Beijing Neurosurgical Institute and Beijing Tiantan Hospital, Capital Medical University, Beijing 100050, China

[5] Department of Radiology and Biomedical Imaging, University of California San Francisco, San Francisco, CA 94143, USA

1 Introduction

EIS is widely adopted as a main treatment for more than 415.5 million patients of cardio-/cerebrovascular diseases worldwide each year [1]. During EIS procedure, the surgeon operates the catheter along vascular lumen to reach the target area inside human body and implements certain surgical tasks such as stent implantation, thrombolysis, and balloon embolization of aneurysm. EIS has its advantages compared with traditional thoracotomy and craniotomy, such as less bleeding, fewer complications, small trauma, quick recovery, and so on [2]. However, EIS still has its drawbacks as follows:

1) Radiological risk to medical staff in EIS is a major concern in medical radiation protection [3]. Although the surgeons always wear a lead apron, glasses, gloves, and so on, the surgeons cannot get full protection [4]. In addition, many surgeons suffer from occupational diseases

Published online: 19 February 2020

like low back pain due to long hours of work wearing heavy lead aprons for radiation protection [5].

2) The surgeon needs to operate the catheter in the narrow space inside the vascular lumen. Even a minor operation mistake might endanger the patient's life.
3) Hands tremor and low operation accuracy of a human surgeon, especially under fatigue condition, will further increase the surgical risk.

Master-slave EIS robotic technology is considered to be a promising way to further improve the operation accuracy and efficiency [6], surgical safety [7–9], and training efficiency of novice surgeons [10, 11]. The surgeon, outside the operating room, can remotely implement the surgical tasks via a master-slave EIS robot to avoid the X-ray radiation. Current researches of EIS robot focus on precisely exerting the expert surgeon's operating skills via the master-slave control architecture. It is one of the most critical issues to accurately detect surgeon's operations through the master controller, which lays the base for precisely controlling the slave robot.

However, the master controllers of current EIS robots commonly adopt rigid-structured operating handles. It is contrary to surgeon's operating habits during conventional EIS, where a surgeon always directly operates a flexible catheter. When using a rigid-structured operating handle, the surgeon must change their habitual operating mode of manipulating a flexible catheter. Although extra training is helpful for the surgeon to get familiar with such rigid-structured operating handles, we consider that, compared with a rigid-structured operating handle, a real catheter as the operating handle can provide more friendly human-machine interaction during robot-assisted EIS.

Although the master controller with rigid handle could realize high-precise detection of surgeon's operation detection, it has its limitation due to the differences with a medical catheter. The master controller using rigid operating handle could be classified into two types, i.e., parallel structure and serial structure. The rigid joystick was commonly adopted as the operating handle by current commercial EIS robotic systems, which is always linked with a parallel-structured pedestal. For instance, Magellan medical vascular catheter control system [12] and Sensei robotic navigation system [13] both employ a three-dimensional hand-operated joystick for the detection of surgeon's operation. CorPath 200 system [14] uses a pair of joysticks as the master controller, though which the surgeon controls the moving direction of the catheter. Through such kind of joystick, only the directions of surgeon's operation (i.e., push, pull, counterclockwise, and clockwise rotation) are detected according to the swing directions of the joystick. The surgeon operates the joystick with swing action in this scenario, which is different with the motion mode of surgeon's hand during conventional EIS. To address this limitation, the haptic interfaces with serial kinematic structure were used as the master controller in our previous researches, such as Geomagic Touch X [15–20] and Phantom Omni [21]. The operator operates the handle with push, pull, and rotate actions to control the slave robot. Such operating mode of surgeon's hands is the same with that in conventional EIS. However, the feeling of surgeon's hand during operating such haptic interfaces is still different with operating a real medical catheter, owing to the rigidity and size differences between the rigid handle and the flexible catheter.

In order to address these problems, several master controllers were developed by taking a medical catheter as the operating handle for surgeon's operation detection. It should be pointed out that the catheter used as the operating handle is not the catheter inserted into human vascular. It is used within the master controller to provide the operator with a high fidelity feeling similar to traditional manual EIS. The surgeon's operation could be detected by measuring the axial and rotational motion of the catheter. Thakur et al. proposed a catheter-motion measuring device [22]. The axial and rotational measurement of the catheter is achieved by mechanically coupling two rotary encoders to the catheter. The catheter's motions are then transformed into detection signal of the rotary encoders. Similar mechanisms were employed in several other EIS robotic systems [23, 24]. A rotary encoder was also used to measure the catheter's motion transmitted through synchronous belt and gears structure [25]. Whether the catheter motions were transmitted to the rotary encoder via rollers mechanism or belt-gear mechanism, sliding between the catheter and the rollers would increase the detection error. In addition, the friction force of mechanical transmission might cause deformation of the catheter, which also increases the detection error.

Noncontact detection methods of catheter's motions show their advantages comparing with above contact detection methods. But the previous noncontact sensing methods still have limitations. The concept "noncontact" here means that the detecting sensor (like camera) does not touch the operating handle (e.g., a real catheter). Current noncontact detection methods of catheter's motions mainly consist of three category: laser sensor-based methods, magnetic sensor-based methods, and image-based methods.

Fukuda et al. use an optical encoder to measure the catheter's motion used for surgeon's skills analysis [26]. The optical encoder consisted of a laser diode, an imaging-process integrated circuit. A laser beam emitted by the diode hits the catheter's surface, and part of it is reflected into the integrated circuit. The optical encoder was calibrated using a magnetic tracker. Yin et al. also developed a similar optical sensing device for catheter motion measurement [27]. A laser-based sensing method was proposed to detect catheter motions [28], where the laser sensor of a wireless mouse is used to acquire catheter surface images. Then the catheter's axial moving distance and rotational distance could be computed basing on

distance output of the wireless mouse. However, the clinical application is not practical due to its high rotational motion detection error (with the standard error of 182.89°comparing with the rotating distance of 1800°).

Fukuda et al. used a magnetic motion capture to track the catheter tip motion for an autonomous catheter insertion robot [29]. Similarly, Rafii-Tari et al. [30] and Chi et al. [31] both employed a six-degree-of-freedom electromagnetic position sensor to measure the catheter tip motion trajectories for data collection. However, the collected data was used for autonomous catheterization model training. The slave robot manipulates the catheter by capturing the catheter end near the sheath out of human body but not the catheter tip inside human body. Furthermore, the motion of catheter tip is no synchronous with the motion of catheter end due to flexibility of the catheter. In addition, even the active controllable catheter can only adjust the orientation of the catheter tip but not the axial displacement. So, the catheter tip motion cannot be directly used for controlling the slave robot.

Some imaging technologies, like radiation-free magnetic resonance (MR) imaging [32] and ultrasound imaging [33] could be promising ways to detect the catheter's motion inside human body for improving surgical safety. Besides, a marker-based detection method was proposed for an EIS virtual-reality training system [34], where the catheter's motions were detected by tracking a marker with four-point groups. Although the rotational actions detection error was reduced by this method compared with Y. Wang's laser-based method [35], its range of axial distance detection was limited by 55 mm. This limitation prohibits the clinical application of this method, because the commonly used clinical catheters are about 1000-mm length. When manipulating such a master controller and arriving at its travel distance limit, the operator must do additional backhaul operations. It will increase the operating time and surgical complexity.

In this paper, a novel continuous noncontact detection method is proposed to detect surgeon's operations toward the master-slave EIS robot. It is enabled by designing a novel sensing device with continuous markers. An optical flow-based corner detection method is used to track the moving marks in a certain computing region. Then, a mathematical model is developed to calculate the axial and rotational displacements of the catheter in three-dimensional (3-D) coordinate system according to the motion information of the detected corners in 2-D image coordinate system. Then, a master controller prototype is developed, and a master-slave EIS robot system is constructed by integrating it with a developed slave robot. Our main contributions are as follows:

(1) We propose a noncontact detection method of EIS surgeon's operation online detection. During master-slave robot-assisted operation, it allows the surgeon still manipulate a real catheter operating handle. Comparing with the rigid operating handle of current commercial haptic interface like Geomagic Touch X [17], a real catheter operating handle matches better with surgeon's habitual operating procedure.
(2) The main shortage of Jin's method is a small axial travel distance limit (55 mm) [34]. But the medical catheter inserting distance commonly achieves more than 1000 mm. We break the axial travel distance limit of their method by introducing continuous chessboard markers and design a novel sensing device.
(3) By comparative simulating experiments in an endovascular evaluator (EVE), we demonstrate that the task completion time with our method is shorter than those with current methods.

The rest of this paper is organized as follows: In Section 2, the overall master-slave EIS robot system is described, and then the proposed continuous noncontact detection method is detailedly illustrated. In Section 3, evaluation experiments and results are described. In Section 4, the experimental results are discussed. In Section 5, the conclusions and future work are drawn.

2 Methodology

2.1 Overview of the master-slave EIS robot system

Surgeon's operation detection plays the critical role for the master-slave EIS robot system, as shown in Fig. 1. During robotic-assisted EIS, the surgeon operates the handle of the master controller while observing the surgical state inside patient's body via digital subtraction angiography (DSA) image. The master controller detects the surgeon's operations in real time and sends the action signals to the slave computer through the master computer. The slave computer generates the control commands according to the received action signals

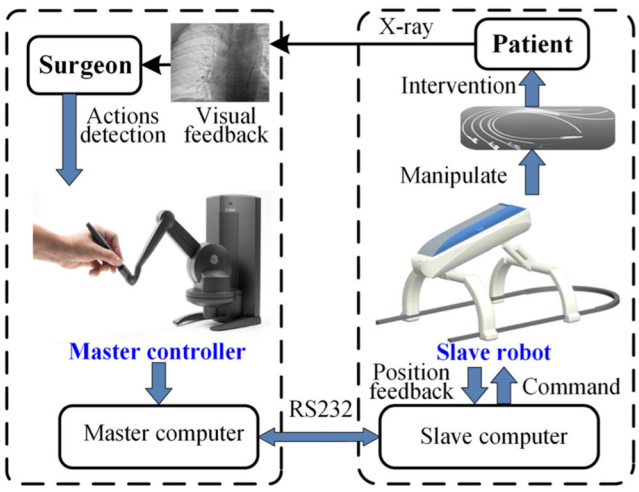

Fig. 1 Framework of the master-slave EIS robot system

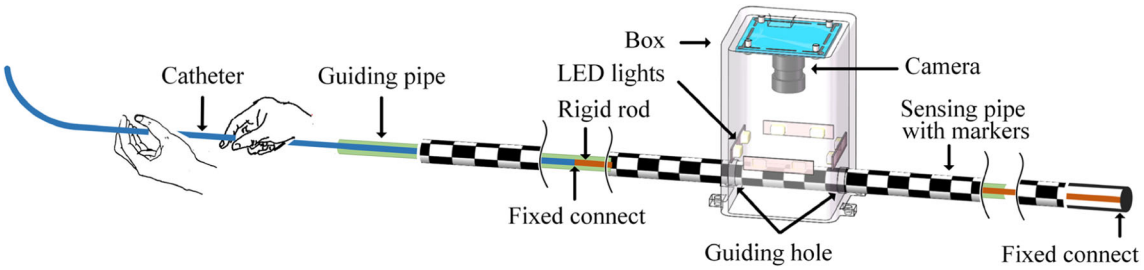

Fig. 2 Schematic diagram of the proposed noncontact detection method and the master controller

and sends them to the motor drivers of the slave robot. The slave robot delivers the catheter tip toward the target point by axial and rotational actions on the catheter end outside human body, which are the same with the surgeon's actions on the operating handle of the master controller. In this master-slave control architecture, the detecting accuracy of the master controller lays the foundation to the final operating accuracy of the catheter. In the following sections, a novel master controller with continuous noncontact detection of surgeon's operation is proposed. Because a real catheter is used as the operating handle, the surgeon's feeling is similar to that in conventional EIS. Also, the proposed detection method breaks the travel distance limit of Jin's marker-based method [34].

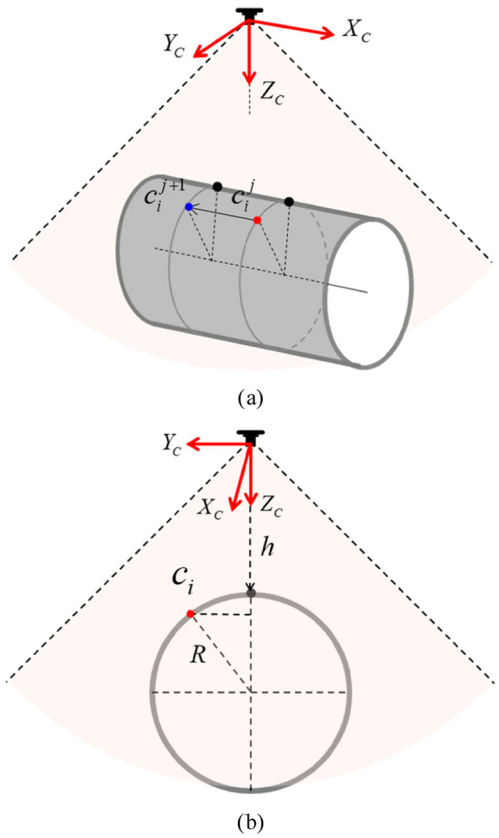

Fig. 3 The axial distance measurement model

2.2 Design of the master controller with proposed detection method

A hypothesis is set for this work that surgeon's operation could be represented by the axial and rotational motion of the catheter. So, the problem of surgeon's operation detection is converted to catheter's axial and rotational moving information detection. In this section, a master controller is designed with a novel noncontact detection method to acquire the catheter's axial and rotational motion in real time.

Figure 2 shows the principle of the detection method and the structure of the designed master controller. The main part of the master controller is designed with concentric tube structure. A medical catheter is used as the operating handle. The catheter goes through a guiding pipe. The guiding pipe is designed to restrain the catheter's deformation. The catheter end is fixed with a rigid rod inside the guiding pipe. The rigid rod also passes through the guiding pipe and then rigidly connected with the end of a sensing pipe. The sensing pipe coaxially covers the guiding pipe. The sensing pipe, together with the inner catheter, rigid rod, and guiding pipe, goes through a pair of guiding holes in a box. A camera is assembled on the top of the box. A group of LED lights inside the box provide the camera with stable illumination condition. When the surgeon operates the catheter, the sensing pipe moves following the catheter driven by the rigid rod fixed with the catheter and the sensing pipe. When the sensing pipe moves following the catheter, the camera acquires the image of the sensing pipe. By tracking the feature points in the image sequence, the moving information of the sensing pipe could be obtained, which represents the motion of the catheter. In J. Guo's detection method [34], only four feature points are tracked due to the limitation of their detection method. The tracked feature points are easy to be missed, which will cause large detection error.

In Jayarathne's method [36], a vision-based pose estimation method is proposed to acquire the 6-D joint pose of an intra-corporeal ultrasound probe. As for the catheter's axial and rotational 2-D motion, this method is quite complex. In this paper, with the pinhole camera model,

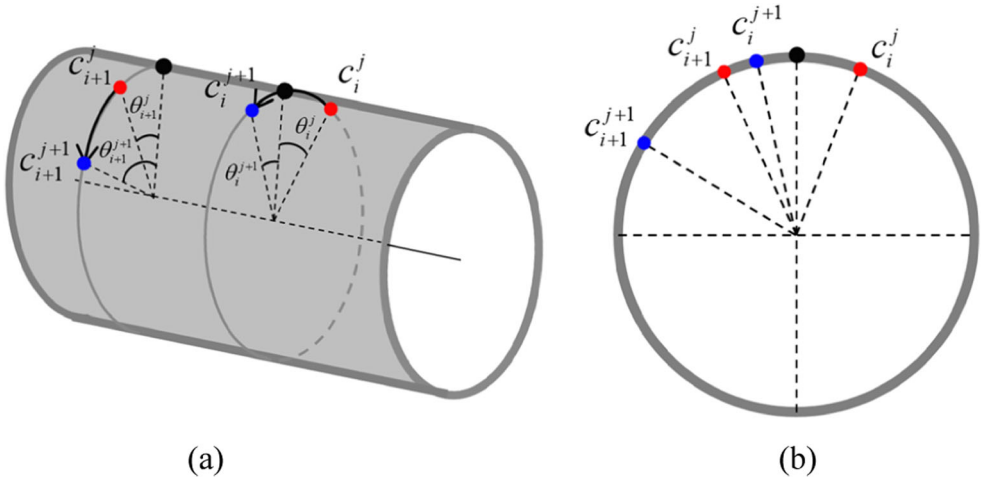

Fig. 4 The rotational angle measurement model

we can get the position of each point on the catheter with high accuracy. In order to acquire plenty of corners, chessboard markers with size of 0.45×0.45 mm are printed on the surface of the sensing pipe, and there are more markers in the camera view. We adopt optical flow algorithm to track more feature points of the markers. By tracking the corner points of the markers on the sensing pipe, the moving information of them could be obtained by optical flow algorithm. Then the moving information of the corner points in 2-D image coordinate system can be transformed into the motion of the sensing pipe in 3-D space in real time by developing a mathematical model.

2.3 Mathematical model of catheter motion

In the proposed detection method, the motion information of the sensing pipe is detected by a monocular camera that can adjust its focal length. Define the coordinates of corner point i in pixel frame as $[u, v]^T$. The coordinates of corner point i in image frame $[x, y]^T$ can be calculated by:

$$\begin{bmatrix} u \\ v \\ 1 \end{bmatrix} = \begin{bmatrix} 1/dx & 0 & u_0 \\ 0 & 1/dy & v_0 \\ 0 & 0 & 1 \end{bmatrix} \begin{bmatrix} x \\ y \\ 1 \end{bmatrix} \tag{1}$$

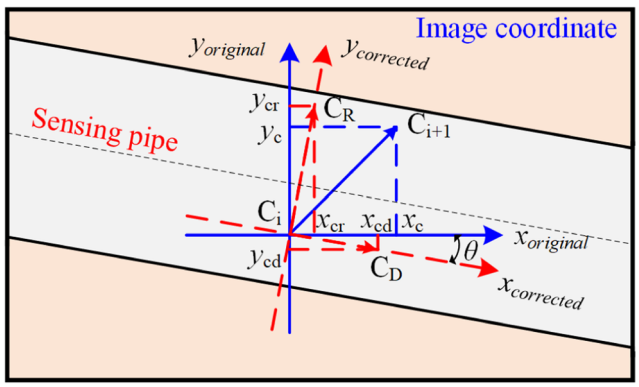

Fig. 5 Schematic of deviation-angle correction model

Because a wide-angle lens is used with the camera for miniaturization of the master controller, the obtained image will generate radial distortion to some extent [37]. In addition, the deviation of the point's coordinates will increase with the point moving away from the center of the image [38]. In order to obtain accurate coordinates of corner point i, it needs to be corrected as follows:

$$\begin{bmatrix} x_c \\ y_c \end{bmatrix} = \left(1 + k_1 r^2 + k_2 r^4 + k_3 r^6\right) \cdot \begin{bmatrix} x \\ y \end{bmatrix} \tag{2}$$

$$\begin{bmatrix} x_c \\ y_c \end{bmatrix} = \begin{bmatrix} x + 2p_1 y + p2\left(r^2 + 2x^2\right) \\ y + p_1\left(r^2 + 2y^2\right) + 2p_2 x \end{bmatrix} \tag{3}$$

where $r^2 = x^2 + y^2$ and $[x_c, y_c]^T$ is the corrected coordinates of corner point i. k_1, k_2, k_3, p_1, and p_2 are distortion coefficients of the camera.

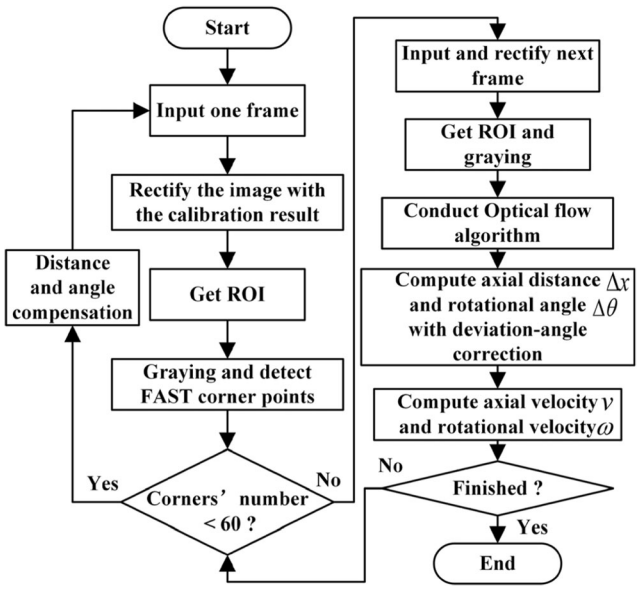

Fig. 6 The flow diagram of the proposed catheter-sensing method

The axial moving distance and rotational angle of corner point i can be obtained by calculating its position difference in adjacent two frames of images, as shown in Fig. 3. The coordinate system of the camera is defined as $O_C-X_CY_CZ_C$. c_i^j ($c_i^j=\left(x_i^j,y_i^j\right)$) is the coordinate of corner point i in frame j, and c_i^{j+1} is the coordinate of corner point i in frame $j+1$. Based on the pinhole imaging principle, the coordinates of corner point i in $O_C-X_CY_CZ_C$ are defined as $P_i^j\left(X_i^j,Y_i^j,Z_i^j\right)$. It can be calculated by:

$$Z_i^j\begin{pmatrix}x_i^j\\y_i^j\\1\end{pmatrix}=\mathbf{M}\begin{pmatrix}X_i^j\\Y_i^j\\Z_i^j\end{pmatrix} \tag{4}$$

where $M=\begin{pmatrix}f&0&0\\0&f&0\\0&0&1\end{pmatrix}$, $Z_i^j=h+R-\sqrt{R^2-\left(Y_i^j\right)^2}$, and h is the distance from the camera to the top point of the catheter.

Then, the axial moving distance of corner point i between frame j and frame $j+1$ can be calculated by:

$$\Delta X^j=\sum_{i=1}^{n}\left(X_i^{j+1}-X_i^j\right) \tag{5}$$

where $n(0<i\le n)$ is the total features number.

As shown in Fig. 4, the rotational angle can be calculated by:

$$\triangle\theta^j=\sum_{i=1}^{n}\left(\arcsin\frac{Y_i^{j+1}}{R}-\arcsin\frac{Y_i^j}{R}\right) \tag{6}$$

where $\arcsin\frac{Y_i^{j+1}}{R}\in\left[-\frac{\pi}{2},\frac{\pi}{2}\right]$.

2.4 Deviation-angle correction model

In order to allow the sensing rod sliding freely through the guiding hole, there is a gap between the sensing rod and the guiding element. A deviation angle between the sensing rod and the guiding hole could be caused by assembling error, as shown in Fig. 5. It leads to motion coupling of feature point in axial direction and rotational direction. In other word, catheter's axial motion causes both feature point displacements along x-axis and y-axis owing to the angle deviation. It is the same to the case of catheter's rotational motion. A correction model is developed in this section to eliminate the effects of the deviation angle on displacement detection accuracy. The deviation angle is defined as θ, which could be obtained by calibration test. Point A_{ti} is the current position of one certain feature point at time ti. And point A_{ti+1} is the position of this feature point at next time step. A_R is the hypothetic position of this feature point at time $ti+1$ only caused by rotation action. A_D is the hypothetic position of this feature point at time $ti+1$ only caused by axial action. Then the displacements y and x caused respectively by axial action and rotational action could be expressed by:

$$\begin{cases}y=y_R/\cos\theta\\x=x_D/\cos\theta\end{cases} \tag{7}$$

$$x=x_D/\cos\theta \tag{8}$$

According to geometrical principle, the following equation set could be obtained:

Table 1 The intrinsic parameters of the camera

Intrinsic parameters			
f_x	f_y	u_0	v_0
551.7462	550.5786	370.0921	220.3538

Table 2 The distortion parameters of the camera

Distortion parameters				
k_1	k_2	k_3	p_1	p_2
0.1034	− 1.3302	3.5957	− 0.00012	− 0.0020

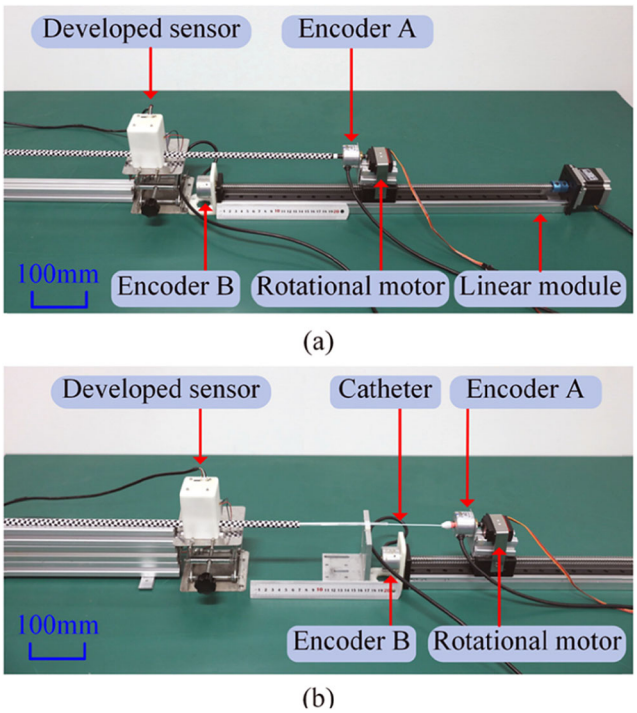

Fig. 7 Experimental setup for calibration and detection accuracy evaluation **a** without catheter and **b** with a medical catheter as the operating handle

Table 3 Summary of the performance in axial motion detection without catheter under different velocities

Velocity (mm/s)	5.76	8.05	10.33	12.62	14.9	17.19
Max. error (mm)	0.72	0.62	0.67	0.75	0.74	0.50
	0.13%	0.11%	0.12%	0.14%	0.13%	0.09%
Mean error	0.36	0.32	0.37	0.31	0.32	0.33
(mm)	0.07%	0.06%	0.07%	0.06%	0.06%	0.06%
Total frames	2282	1171	1362	1138	974	793

$$\begin{cases} x_A = x_R + x_D \\ y_A = y_R + y_D \\ x_R = y_R \cdot \tan\theta \\ y_D = x_D \cdot \tan\theta \end{cases} \tag{9}$$

y_R and x_D could be calculated by solving:

$$\begin{cases} y_R = (y_A - x_A \cdot \tan\theta)/(1 - \tan\theta) \\ x_D = x_A - (y_A - x_A \cdot \tan\theta) \cdot \tan\theta/\left(1 - \tan^2\theta\right) \end{cases} \tag{10}$$

Then the displacements y and x caused respectively by axial action and rotational action could be expressed by:

$$\begin{cases} y = (y_A - x_A \cdot \tan\theta)/[(1 - \tan\theta) \cdot \cos\theta] \\ x = x_A - (y_A - x_A \cdot \tan\theta) \cdot \tan\theta/\left[\left(1 - \tan^2\theta\right) \cdot \cos\theta\right] \end{cases} \tag{11}$$

2.5 Real-time detection algorithm

The flow diagram of our real-time detection algorithm is shown in Fig. 6. The first step is to input one frame and rectify the image with the calibration parameters. Then get the region of interest (ROI) with certain size for detecting the feature points on sensing pipe. Calculating only within ROI reduces the computation. The rectified ROI is transformed into grayscale images, and a FAST (features from accelerated segment test) corner detector [37] is used to extract the features on the sensing pipe surface. In order to achieve accurate detection, the sub-pixel coordinate values of these corners are calculated by interpolating the intensity surrounding the pixel coordinates of features. In our proposed method, in order to keep the robustness, FAST features will not update until the corner points' number is less than 60. When the corner points' number is large than 60, optical flow algorithm is used to track the corner points using rectified grayscale ROI of next frame. In this way, the motion of the sensing pipe is obtained with the coordinate of corner points in two frames. During the time t for FAST features update and the sub-pixel coordinate calculation, the motion of the sensing pipe is not calculated. It will cause detection error. So, it is necessary to compensate the lost distance. The compensated axial distance Δx and rotational angle $\Delta\theta$ can be calculated according to the current axial velocity v and rotational velocity ω and time t, which can be expressed by (12).

$$\begin{cases} \Delta x = v \times t \\ \Delta\theta = \omega \times t \end{cases} \tag{12}$$

Table 4 Summary of the performance in rotational motion detection without catheter under different angular velocities

Velocity (°/s)	50	60	70	80
Max. error(°)	13.72	10.23	13.26	7.44
	1.25%	0.93%	1.21%	0.68%
Mean error(°)	6.36	3.28	6.36	4.05
	0.58%	0.30%	0.58%	0.37%
Total frames	546	451	389	340

3 Evaluation experiments and results

In this section, the developed master controller is calibrated firstly. The calibration results are show in Tables 1 and 2. The camera calibration errors are 0.1155 and 0.1141 pixel, respectively, along x and y directions, which is acceptable for the catheter motion sensing. Second, the detection accuracy of the developed sensor is evaluated under standard condition. Finally, an EIS robot system is developed by integrating a prototype of the master controller and a developed slave robot. Basing on the EIS robot system, tests of a basic catheter insertion task are conducted in an EVE to evaluate the performance of the developed master controller.

3.1 Evaluation of detection accuracy

Firstly, in order to avoid the effects of the catheter deformation, evaluation experiments without the catheter are conducted using the experimental setup shown in Fig. 7a. The developed master controller is fixed on the test bed. The linear module is used to drive the sensing pipe along axial direction. The axial moving distance is set to be 550 mm. And, the electric actuator is used to drive the sensing pipe along circumferential direction. The rotational moving angle is set to be 1100°. The sensing pipe of the developed sensor is directly fixed with the shaft of the electric actuator. The axial distance and rotational angle of the sensing pipe detected respectively by encoder A and encoder B (HK50, made by Shenzhen HZJ Co., Ltd., CN) are used as the true distance values for

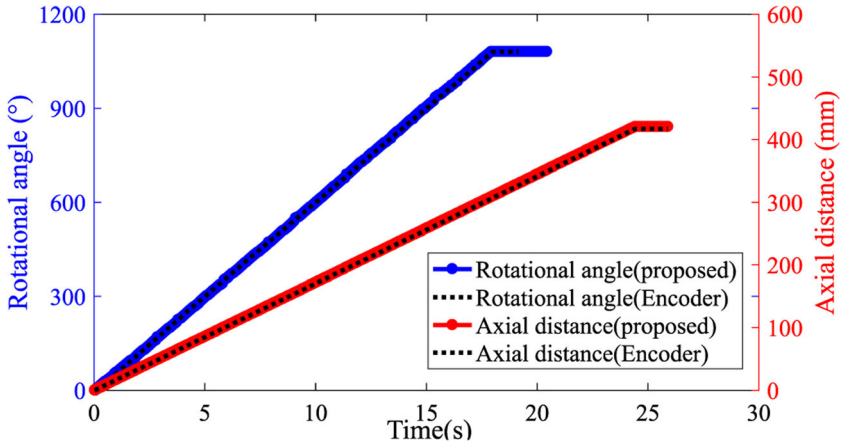

Fig. 8 Axial and rotational moving distance without the catheter in one test

detection error evaluation. Each experiment is repeated by 10 times for statistical analysis.

The statistical results of the axial motion detection error without the catheter are shown in Table 3. The axial motion velocities of the sensing pipe range from about 6 to 17 mm/s. The mean axial motion detection errors under different axial motion velocities range from 0.31 to 0.36 mm. The relative mean axial motion detection errors range from 0.06 to 0.07%. The maximum axial motion detection errors vary from 0.5 to 0.75 mm, and the relative maximum errors are from 0.09 to 0.14%. The maximum standard deviation of axial motion detection error is 0.44 mm. Table 4 shows the statistical results of rotational motion detection error. The rotational angle velocities of the sensing pipe range from 50°/s to 80°/s. The mean rotational detection errors with different rotational angel velocities range from 3.2° to 6.3°. The relative mean rotational motion detection errors range from 0.29 to 0.57%. The maximum rotational motion detection errors vary from 7.44° to 13.72°, and the relative maximum errors are from 0.68 to 1.25%. The maximum standard deviation of rotational motion detection error is 7.35°. The axial and rotational moving distances during one representative test are shown in Fig. 8. It can be seen that the curve of the axial and rotational moving distances detected by the proposed master controller fits well with those of the standard value recorded by encoder A and encoder B.

Secondly, using the experimental setup shown in Fig. 7b, experiments are conducted with the whole master controller to evaluate its detection performance combining the effects of the catheter deformation. A clinical catheter (with size of 5f) of the developed master controller is fixed to the shaft of the electric actuator. Two groups of experiments are designed. The length of the catheter between the fixing point with the electric actuator and the fixing point with the rigid rod inside the master controller is respectively set to be 100 mm and 400 mm. The catheter is driven with axial driving velocity of about 10 mm/s and rotational velocity of about 65°/s. The axial moving distance is set to be 73 mm. And, the electric actuator is used to drive the sensing pipe along circumferential direction. The rotational moving distance is set to be 460°. Each group of experiments is repeated by 10 times.

Table 5 Summary of the performance in axial and rotational motion detection with catheter under different velocities

Catheter length (mm)		10	40
Max. error	Axial motion (mm)	0.31(0.43%)	0.41(0.56%)
	Rotational motion (°)	7.01(1.52%)	8.60 (1.87%)
Mean error	Axial motion (mm)	0.22(0.3%)	0.31(0.42%)
	Rotational motion (°)	4.04(0.88%)	4.79 (1.04%)
Total frames		210	215

The results of axial distance detection error and rotational angle detection error are shown in Table 5. The mean and maximum detection errors of axial distance with catheter length of 100 mm are 0.22 mm and 0.31 mm, and the relative mean and maximum axial distance detection errors are 0.30% and 0.43%. The mean and maximum rotational angle detection error with catheter length of 100 mm is 4.04° and 7.01°, and the relative mean and maximum rotational angle detection errors are 0.88% and 1.52%. The mean and maximum detection error of axial distance with catheter length of 400 mm is 0.31 mm and 0.41 mm, and the relative mean and maximum detection error is 0.31% and 0.41%. The mean and maximum rotational angle detection error with catheter length of 400 mm is 4.79° and 8.60°, and the relative mean and maximum rotational angle detection error is 1.04% and 1.87%. The detection errors with catheter are at the same level of those without the catheter. It means that the catheter deformation is smaller enough and causes no effect on detection accuracy. The results of axial distance and rotational angle in one representative test with catheter length of 400 mm are shown in Fig. 9. It can be seen that the curve of the axial and rotational moving distances detected by the proposed master controller fits well with those of the standard value recorded by encoder A and encoder B. From these experiments, all total frames are recorded, and the frame per second is up to 25 Hz, which

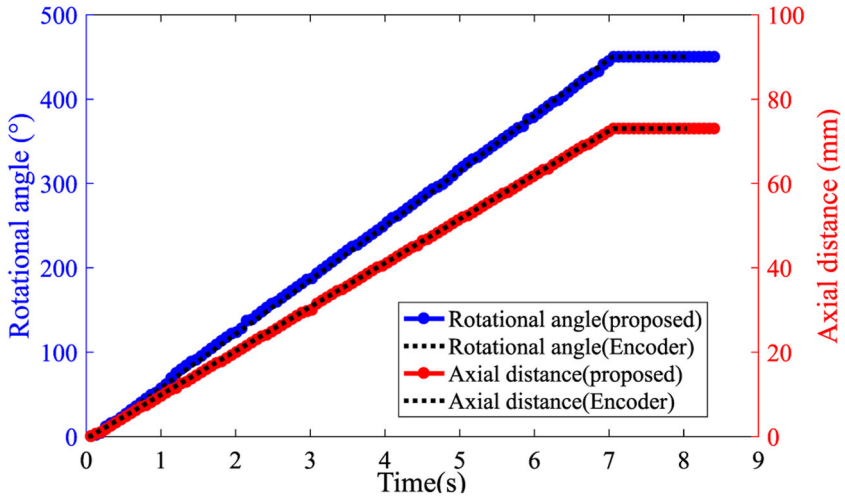

Fig. 9 Axial and rotational moving distance with the catheter in one test

proved that the proposed method has high real-time performance.

We further conduct a comparison between our method and other research works, as shown in Table 6. Comparing with the commercial Geomagic® Touch X, although the axial and rotational detection errors are relatively larger, there is no axial and rotational travel distance limit for our method. When a surgeon manipulates the handle of Geomagic® Touch X and arrives at its travel distance limit, they must do additional backhaul operations to control the slave robot continuously inserting the catheter. It will interrupt the surgeon's normal operation. Wang's method also has no axial and rotational travel distance limit, but both of its axial and rotational detection error are much larger than our method. Jin's method also employed a camera to tracking for marker to measure the catheter's motion, but its rotational detection error is much larger than our method.

In addition, it also has axial travel distance limit of 55 mm, which is even smaller than Geomagic® Touch X. So, our method achieves better overall performance for EIS surgeon's operation action detection, compare with Jin's method, Wang's method, and Geomagic® Touch X.

3.2 Evaluation of surgical-task implementing performance

A master-slave EIS robot is constructed by integrating the developed master controller and a slave EIS robot, as shown in Fig. 10a. The inner structure of the slave robot is shown in Fig. 10b. Axial motion and rotational motion of the catheter are realized respectively by the axial unit and the rotational unit. The axial unit mainly consists of a servomotor (SGMJV-01ADE6S, made by Yaskawa Electric Corporation, Ltd., JP) and a ball screw (SKR/KR26, with the travel distance of 240 mm, made by THK Co., Ltd., JP). The servomotor drives the sliding block moving along axial direction.

The rotational unit and the clamping device are fixed with the sliding block. The rotational unit mainly consists of a DC motor (EC-max 16 and a driver of EISCON 50/5, all made by Maxon Co., Ltd., JP) and a herringbone gear pair. The clamping device, including a designed clamping mechanism

Table 6 Comparison between our method and current methods

Method	Operating handle	Basic principle	Axial relative error	Rotational relative error	Axial travel distance limit	Rotational travel distance limit
Our method	Real catheter	Camera Montinous marker Noncontact	0.061%	0.46%	None (100% length of real catheter)	None
Jin et al. [34]	Real catheter	Camera marker Noncontact	0.03%	3.55%	55 mm (about 5.5% length of real catheter)	None
Wang et al. [35]	Real catheter	Laser mouse sensor Noncontact	3.2%	10.05%	None (100% length of real catheter)	None
Bao et al. [17]	Rigid rod of commercial Geomagic® Touch X	Motor and encoder Contact	0.01% Resolution	±3% Linearity	160 mm (about 16% length of real catheter)	304°

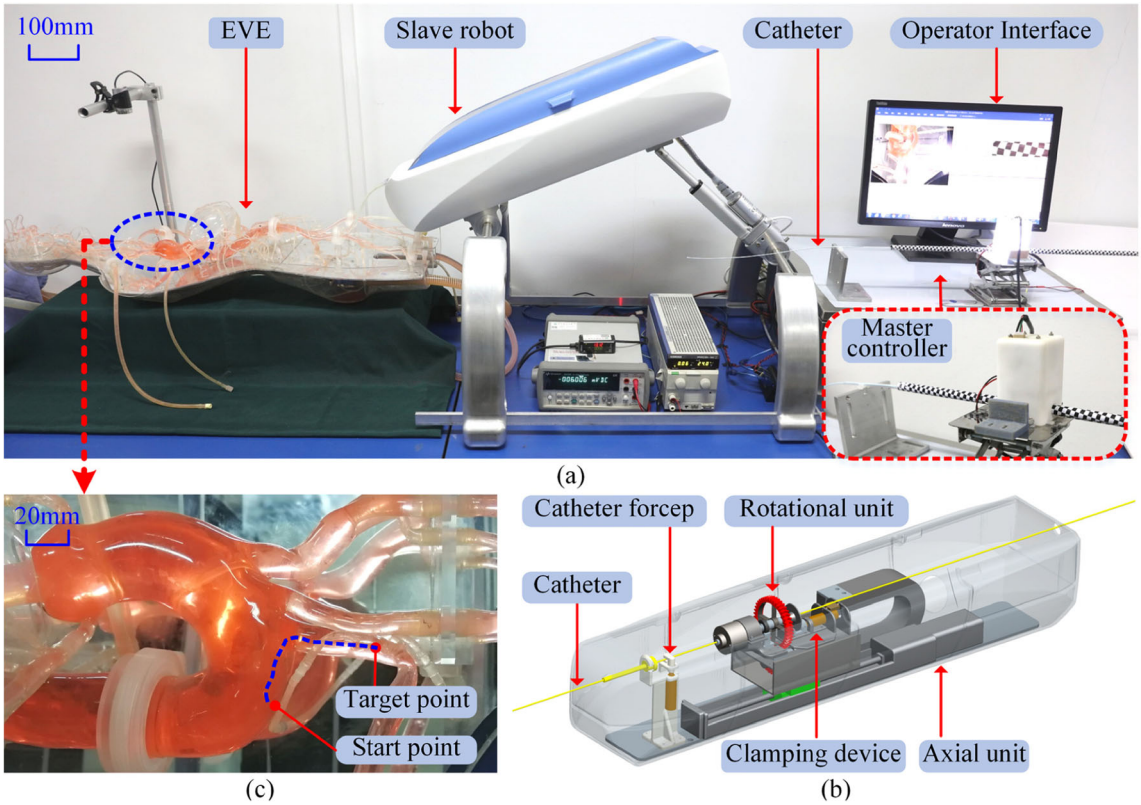

Fig. 10 Experimental setups for surgical task implementation. **a** The developed master-slave EIS robot, **b** inner structure of the slave robot, and **c** magnification of the surgical path in EVE

and a DC electromagnet, is fixed with the axis of the driven gear of the herringbone gear pair. The motion principle of the slave robot can be described as follows: Drive the clamping device to clamp the catheter. Then drive the sliding block of the ball screw to operate the catheter along axial direction and the herringbone gear pair to operate the catheter along rotational direction. When the maximum ball screw travel distance of the manipulator reaches, lose the clamping device, electrify the catheter forceps to fix the catheter, and withdraw the catheter following the sliding block. The clamping forceps is actuated by a DC electromagnet. When the sliding block arrives at the starting point of the ball screw, clamp the catheter or guidewire again. Then, repeat the above steps until the catheter tip reaches the target point. An operator visual interface is designed to provide the operator with the image of cathetering situation inside the vascular model.

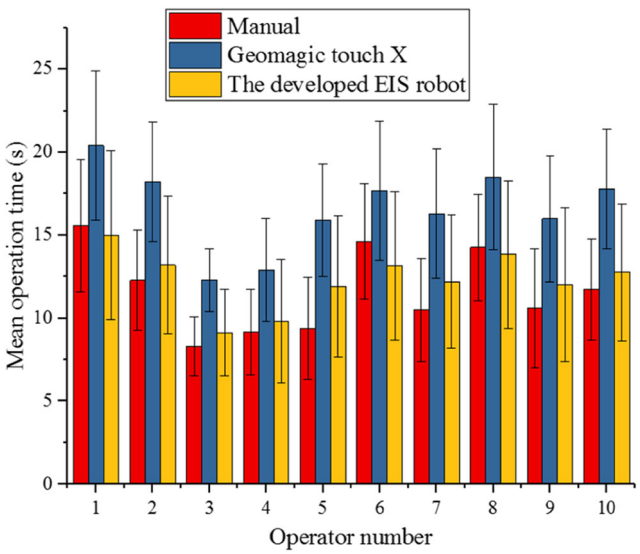

Fig. 11 Results of operation time for surgical task implementation

The experimental surgical task in EVE is designed as follows: The catheter tip is initially located at the starting point inside the aortic arch as shown in Fig. 10c. The operator needs to control the slave robot via the master controller to push, pull, and rotate the catheter to deliver its tip to the target point inside the left subclavian vein. Ten operators are employed to repeat the designed surgical task by ten times. In addition, every operator is asked to implement the surgical task manually and with Geomagic Touch X, respectively. And every operator tries ten times. Before formal experiments, every operation could try five times of the given task operation. For quantitative analysis, the operating time of every task implementation, operation of the operator, and images of the cathetering situation are recorded. The operating time is a critical evaluation index for EIS. Shorter operating time indicates less X-ray damage and less possibility of vascular damage.

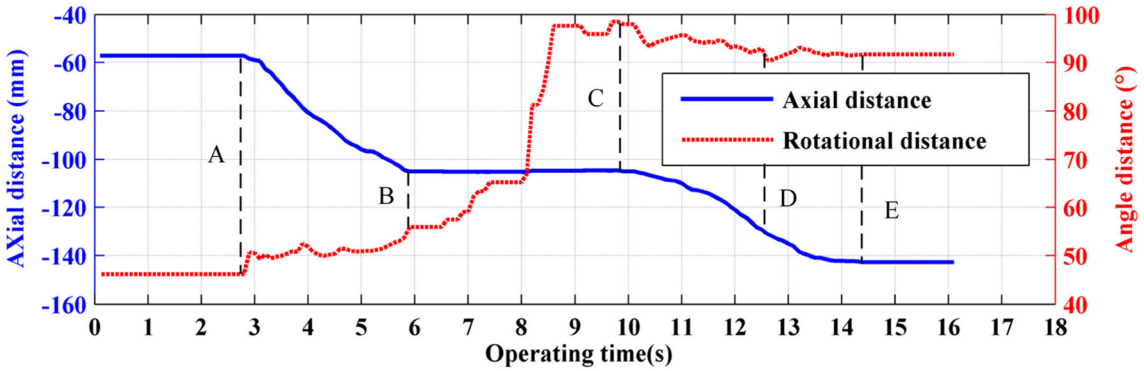

Fig. 12 Moving distance of the catheter proximal end in one test

The results of operating time are shown in Fig. 11. The operation time of robot-assisted operations range from 9.1 to 15.0 s, the manual operations range from 8.3 to 15.56 s, and the operations with Geomagic Touch X vary from 12.3 to 20.4 s. The mean operation time with the proposed EIS robot are at the same level with those of manual operation. Compared with operation with Geomagic Touch X, the operation time of the developed EIS robot decreases 25.7%, which indicates the superiority of the developed EIS robot. In addition, the deviations of operation time with the developed EIS robot range from 2.6 to 5.1 s, and those of manual operation range from 1.7 to 3.9 s. For 7 of the ten operators, the mean operation time of manual operations are shorter than those of robot-assisted operation. In contrast, for the other 3 operators, the mean operation time of manual operations are relatively larger. It indicates that these 3 operators are more adaptive to the manner of robot-assisted operation compared with the other 7 operators.

The detailed operating procedure of one representative test is shown in Figs. 12 and 13. Figure 12 shows the operator's operation at several critical moments, which are represented by the detected axial distance and rotational distance of operation via the master controller. The times A to E in Fig. 12 are corresponding to the frames (a) to (e) in Fig. 13. At time A, the catheter tip locates at the starting point, and the operator starts to push forward the catheter. At time B, the catheter tip arrives at the junction of the aortic arch and the left subclavian vein. The operator stops pushing the catheter and rotates the catheter tip toward the entrance of the left subclavian vein. At time C, the catheter tip gets into the entrance of the left subclavian vein. The operator stops rotating the catheter and starts to push forward the catheter. At time D, the catheter is inserted into the left subclavian vein by a distance, and the operator continuously pushes the catheter toward the target point. At time E, the catheter reaches the target point, and the operator stops operating the catheter.

4 Discussion

The experimental results indicate that the proposed master controller successfully realizes continuous noncontact detection of the operators' operation during simulated surgical task implementation. Compared with the laser-mouse-based noncontact detection method [35], the rotational detection error is reduced by 92.5%. Compared with the marker-based noncontact detection method [34], the limitation of axial detecting range is broken. In the experiments, the axial detection range is 10 times larger than the detection range of the marker-based noncontact detection method. Theoretically, these are no limitation of axial and rotational detecting range for the proposed continuous noncontact detection method. In addition, despite the absolute axial operation detection error of the proposed method is at the same level with the marker-based noncontact

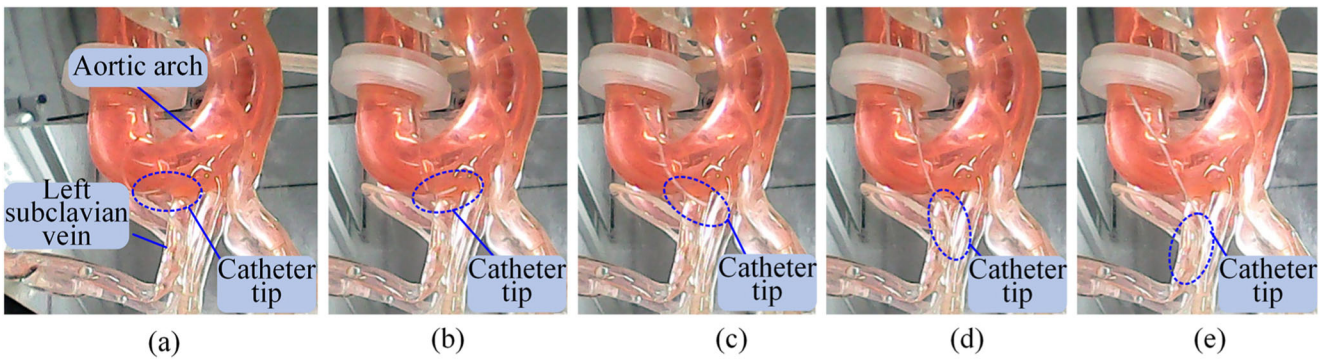

Fig. 13 Moving procedure of the catheter tip in the test. The frames (**a**) to (**e**) are corresponding to time A to E in Fig. 12

detection method, the relative detection error is reduced by 77%. The relative rotational detection error with the proposed method is 98.5% smaller than those with the marker-based noncontact detection method.

The detection error is mainly caused by the tracking error of corners. Because of the gap and friction force between the sensing pipe and guiding hole, crawl phenomenon of the sensing pipe is observed when it moves through the guiding hole. Because a fixed deviation angle of the developed master controller is used for calculation, the deviation-angle correction model could not completely solve the error caused by the deviation. However, it could be solved by replacing the sliding pairs by the rolling pairs in further optimized mechanism. Also, the drift in the input pose over time would be one of the main factors that increasing the detecting error of the device. It would lead to potential surgical risk. ArUco marker [39] could be used to solve this problem, of which the absolute position on the sensing pipe can be known. We could use this absolute position for online calibrating to reduce the risk caused by corner point detecting drift.

Comparative result shown in Fig. 11 indicates that the proposed master controller with noncontact detection method is superior than Geomagic Touch X from the point of operation time. Compared with the Geomagic Touch X with rigid operating handle, the developed master controller takes the medical catheter as the operating handle. The most significant advances of the proposed master controller with the medical catheter are realizing continuous noncontact detection and providing the operator with high-fidelity human-machine interaction similar to manual EIS procedure.

More complete high-fidelity human-machine interaction could be achieved by combining the proposed master controller with certain force feedback generating device, such as magnetorheological (MR) fluids-based haptic interface [27]. In this way, the catheter operating force detected by the slave robot could be fed back to the operator via the catheter operating handle. Real-time sensing of catheter operating force could enhance the surgery safety of robot-assisted EIS.

5 Conclusion

In this paper, a novel master controller with vision-based detection of surgeon's operation is proposed for the EIS robot. A continuous noncontact detection method is proposed for real-time detection of surgeon's operation. The clinical catheter is sued as the operating handle, which is consistent with the surgeon's habit during traditional EIS. It provides the operator with high fidelity of human-machine interaction.

(1) A prototype of the proposed master controller is developed for detecting performance evaluation. The results demonstrate that the proposed detection method surpasses the current surgeon's operation detection method from the point of view of measuring range of axial motion and detecting accuracy.
(2) The results of surgical task implementation experiments in EVE indicate that the developed master controller performs well for controlling of the salve robot during simulated tests.
(3) In the future work, the detecting accuracy could be increased by optimizing the structure of the sensing pipe guiding mechanism and eliminating the effect of corner point detecting drift using ArUco marker [39]. In addition, compatible force feedback device should be studied to be combined with the proposed master controller to enhance the surgery safety.

Funding information This research is partly supported by National High-tech R&D Program (863 Program) of China (No. 2015AA043202) and National Key Research and Development Program of China (2017YFB1304401).

References

1. Roth G, Johnson C, Abajobir A (2017) Global regional and national burden of cardiovascular diseases for 10 causes 1990 to 2015. J Am Coll Cardiol 70(1):1–25
2. Dankelman J, Dobbelsteen J, Breedveld P (2010) Current technology on minimally invasive surgery and interventional techniques. Paper presented at the 2010 IEEE international conference on instrumentation control and automation 12-15
3. Oonsiri S, Jumpangern C, Sanghangthum T (2007) Radiation dose to medical staff in interventional radiology. J Med Assoc Thail 90(4):823–828
4. Kamusella P, Scheer F, Ludtke CW (2017) Interventional angiography: radiation protection for the examiner by using lead-free gloves. J Clin Diagn Res 11(7):C26–C29
5. Naito N (2005) Occupational back pain in the interventional radiologist. J Vasc Interv Radiol 16(2):312–314
6. Kim Y, Cheng S, Diakite M, Gullapalli R, Simard J, Jaydev JD (2017) Toward the development of a flexible mesoscale MRI-compatible neurosurgical continuum robot. IEEE Trans Robot 33(6):1386–1397
7. Vandini C, Bergeles B, Glocker P, Giataganas YG (2017) Unified tracking and shape estimation for concentric tube robots. IEEE Trans Robot 33(4):901–915
8. Zhang L, Guo S, Yu H, Song Y (2017) Performance evaluation of a strain-gauge force sensor for a haptic robot-assisted catheter operating system. Microsyst Technol 23(10):5041–5050
9. Guo J, Guo S, Yu Y (2016) Design and characteristics evaluation of a novel teleoperated robotic catheterization system with force feedback for vascular interventional surgery. Biomed Microdevices 18: 76. https://doi.org/10.1007/s10544-016-0100-0
10. Guo J, Guo S, Tamiya T, Hirata H, Ishihara H (2014) A virtual reality-based method of decreasing transmission time of visual feedback for a tele-operative robotic catheter operating system. Int J Med Robot Comput Assisted Surg 12(1):32–45
11. Vitiello V, Kwok K, Yang G (2012) Medical robotics: minimally invasive surgery (1st ed). Woodhead Publishing Series in Biomaterials

12. Rao S (2016) Endovascular robotic catheters: an emerging transformative technology in the interventional radiology suite. J Radiol Nurs 35(3):211–217. https://doi.org/10.1016/j.jradnu.2016.04.022
13. Antoniou G, Riga C, Mayer E, Cheshire N, Bicknell C (2011) Clinical applications of robotic technology in vascular and endovascular surgery. J Vasc Surg 53(2):493–499. https://doi.org/10.1016/j.jvs.2010.06.154
14. Granada J, Delgado J, Uribe M, Fernandez A, Blanco G, Leon M, Weisz G (2011) First-in-human evaluation of a novel robotic-assisted coronary angioplasty system. J Am Coll Cardiol Intv 4(4):460–465. https://doi.org/10.1016/j.jcin.2010.12.007
15. Zhao Y, Guo S, Xiao N, Wang Y, Li Y, Jiang Y (2018) Operating force information on-line acquisition of a novel slave manipulator for vascular interventional surgery. Biomed Microdevices 20:33. https://doi.org/10.1007/s10544-018-0275-7
16. Bao X, Guo S, Xiao N, Li Y, Yang C, Shen R, Cui J, Jiang Y, Liu X, Liu K (2018) Operation evaluation in-human of a novel remote-controlled vascular interventional robot. Biomed Microdevices 20:34. https://doi.org/10.1007/s10544-018-0277-5
17. Bao X, Guo S, Xiao N (2018) Compensatory force measurement and multimodal force feedback for remote-controlled vascular interventional robot. Biomed Microdevices 20:74–11. https://doi.org/10.1007/s10544-018-0318-0
18. Guo S, Wang Y, Xiao N, Li Y, Jiang Y (2018) Study on real-time force feedback for a master–slave interventional surgical robotic system. Biomed Microdevices 20:37
19. Yang C, Guo S, Bao X, Xiao N, Shi L, Li Y, Jiang Y (2019, 2019) A vascular interventional surgical robot based on surgeon's operating skills. Med Biol Eng Comput:1–12. https://doi.org/10.1007/s11517-019-02016-8
20. Zhao Y, Guo S, Wang Y, Cui J, Ma Y, Zeng Y, Liu X, Jiang Y, Li Y, Shi L, Xiao N (2019) A CNNs-based prototype method of unstructured surgical state perception and navigation for an endovascular surgery robot. Med Biol Eng Comput 57:1875–1887. https://doi.org/10.1007/s11517-019-02002-0
21. Lu W, Xu W, Zhang J, Liu D, Wang D, Jia P, Li Z, Wang T, Zhang D, Tian Z, Zeng Y (2011) Application study of medical robots in vascular intervention. Int J Med Robot Comput Assisted Surg 13(3). https://doi.org/10.1002/rcs.406
22. Thakur Y, Cakiroglu JH, Holdsworth DW, Drangova M (2007) A device for real-time measurement of catheter-motion and input to a catheter navigation system. SPIE. https://doi.org/10.1117/12.709556
23. Zhou C, Xie L, Shen X, Luo M, Wu Z, Gu L (2015) Cardiovascular interventional surgery virtual training platform and its preliminary evaluation. Int J Med Robot Comput Assisted Surg 11(3):375–387. https://doi.org/10.1002/rcs.1627
24. Zhang L, Guo S, Yu H, Song Y, Tamiya T, Hirata H, Ishihara H (2018) Design and performance evaluation of collision protection-based safety operation for a haptic robot-assisted catheter operating system. Biomed Microdevices 20(2):22. https://doi.org/10.1007/s10544-018-0266-8
25. Song Y, Guo S, Yin X, Zhang L, Hirata H, Ishihara H, Tamiya T (2018) Performance evaluation of a robot-assisted catheter operating system with haptic feedback. Biomed Microdevices 25:50–16. https://doi.org/10.1007/s10544-018-0294-4
26. Tercero C, Kodama H, Shi C, Ooe K, Ikeda S, Fukuda T, Arai F, Negoro M, Kwon G, Najdovski Z (2013) Technical skills measurement based on a cyber-physical system for endovascular surgery simulation. Int J Med Robot Comput Assisted Surg 9(3):e25–e33. https://doi.org/10.1002/rcs.1467
27. Yin X, Guo S, Xiao N, Tamiya T, Hirata H, Ishihara H (2016) Safety operation consciousness realization of a MR fluids-based novel haptic interface for teleoperated catheter minimally invasive neurosurgery. IEEE/ASME Trans Mechatron 21(2):1043–1054. https://doi.org/10.1109/TMECH.2015.2489219
28. Wang Y, Guo S, Tamiya T, Hirata H, Ishihara H, Yin X (2016) A virtual reality simulator and force sensation combined catheter operation training system and its preliminary evaluation. Int J Med Robot Comp 13:e1769. https://doi.org/10.1002/rcs.1769
29. Tercero C, Ikeda S, Uchiyama T, Fukuda T, Arai F, Okada Y, Ono Y, Hattori R, Yamamoto T, Negoro M, Takahashi I (2007) Autonomous catheter insertion system using magnetic motion capture sensor for endovascular surgery. Int J Med Robot Comput Assisted Surg 3(1):52–58. https://doi.org/10.1002/rcs.116
30. Rafiii H, Liu J, Lee S, Bicknell C, Yang G (2013) Learning-based modeling of endovascular navigation for collaborative robotic catheterization. International Conference on Medical Image Computing and Computer-assisted Intervention 369-377. https://doi.org/10.1007/978-3-642-40763-5_46
31. Chi W, Liu J, Rafii H, Riga C, Bicknell C, Yang G (2018) Learning-based endovascular navigation through the use of non-rigid registration for collaborative robotic catheterization. Int J Comput Ass Rad 13(6):855–864. https://doi.org/10.1007/s11548-018-1743-5
32. Koolwal AB, Barbagli F, Carlson C, Liang D (2010) An ultrasound-based localization algorithm for catheter ablation guidance in the left atrium. Int J Robot Res 29(6):643–665
33. Chen F, Liu J, Liao H (2016) 3D catheter shape determination for endovascular navigation using a two-step particle filter and ultrasound scanning. IEEE Trans Med Imaging 36(3):685–695
34. Guo J, Guo S, Li M, Tamiya T (2018) A marker-based contactless catheter-sensing method to detect surgeons' operations for catheterization training systems. Biomed Microdevices 20(3):76. https://doi.org/10.1007/s10544-018-0321-5
35. Wang Y, Guo S, Yin X (2015) Laser mouse-based master-slave catheter operating system for minimally invasive surgery. Proceedings of 2015 IEEE international conference on mechatronics and automation, Beijing, China
36. Jayarathne UL, Luo X, Chen ECS, Peters TM (2015) Simultaneous Estimation of Feature Correspondence and Stereo Object Pose with Application to Ultrasound Augmented Robotic Laparoscopy the Workshop on Augmented Environments for Computer-Assisted Interventions 9365
37. Bosch J, Gracias N, Ridao P, Ribas D (2015) Omnidirectional underwater camera design and calibration. Sensors 15(3):33–65
38. Kannala J, Brandt S (2006) A generic camera model and calibration method for conventional, wide-angle, and fish-eye lenses. IEEE Trans Pattern Anal Mach Intell 28:1335–1340
39. Huang B, Ye M, Hu Y et al (2018) A Multi-Robot Cooperation Framework for Sewing Personalized Stent Grafts. IEEE Trans Ind Inf 14(4):1776–1785

Yan Zhao was born in Hebei, China, in 1988. He is currently a lecturer in School of Hebei University of Technology, China. He received the Ph.D. from Beijing Institute of Technology in 2019. He received the B.Sc and M.sc from Hebei University of Technology, China, in 2012 and 2015. His research interests include surgical robotics, machine learning, biomedical engineering, and mechanical engineering.

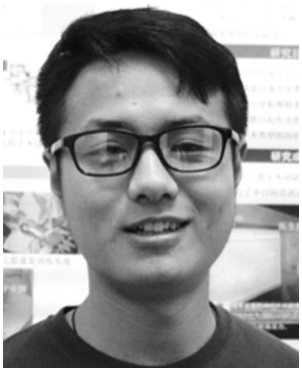

Yuxin Wang was born in Anhui, China, in 1996. He is currently pursuing the master's degree in biomedical engineering with School of Life Sciences, Beijing Institute of Technology, China. He received the B.Sc in automation from Beijing Institute of Technology, China. His research interests include surgical robotics, machine learning, and biomedical engineering.

Huiming Xing was born in Shandong, China, in 1988. He received the B.S. degree in automation from Qilu University of Technology, China, in 2013 and the M.sc in automation from Harbin Engineering University, China, in 2016. He is currently pursuing the doctor's degree in automation at Beijing Institute of Technology, China. His current research interests include amphibious robot, computer vision, and multi-robot cooperation.

Jinxin Cui was born in Shandong, China, in 1995. She is currently pursuing the master's degree in biomedical engineering with School of Life Science, Beijing Institute of Technology, China. She received the B.Sc from Beijing Institute of Technology. Her research interests include biomedical engineering, surgical robotics, and machine learning.

Shuxiang Guo was born in Jilin, China, in 1963. He received the Ph.D. degree from Nagoya University in 1995. He is currently a professor in biomedical engineering at Beijing Institute of Technology and Kagawa University, Japan. He is the leader of Key Laboratory of Convergence Biomedical Engineering System and Healthcare Technology, The Ministry of Industry and Information Technology, China. He is the Editor in Chief of IJMA (International Journal of Mechatronics and Automation). His research interests include surgical robotics, rehabilitation robotics, endoscopic capsule robotics, and underwater robotics.

Youchun Ma was born in Heilongjiang, China, in 1996. He is currently pursuing the master's degree in biomedical engineering with School of Life Sciences, Beijing Institute of Technology, China. He received the B.Sc in automation from Hebei University of Technology, China. His research interests include surgical robotics, machine learning, biomedical engineering, and automation.

Yu Liu was born in Shanxi, China, in 1997. She received the B.Sc in biomedical engineering from Beijing Institute of Technology, China, in 2017. She is currently pursuing the master's degree in biomedical engineering with Beijing Institute of Technology, China. Her current research interests include indoor localization, sensor fusion, path planning, and computer vision.

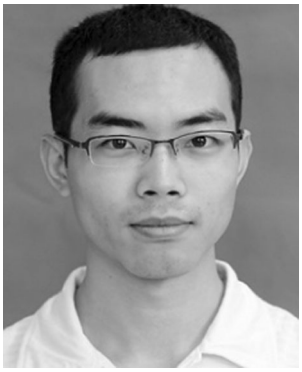

Junqiang Feng was born in 1993. He received the B.Sc in Hebei Medical University in 2016. He is receiving his resident training at Beijing Tiantan Hospital, Capital Medical University. His major interest includes endovascular surgery robotic system clinical experiment and black blood imaging and hemodynamic study of intracranial aneurysms.

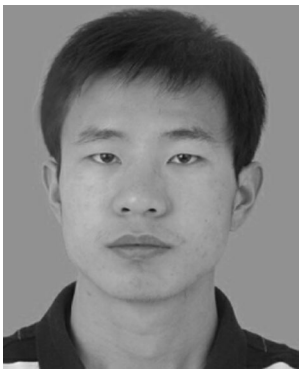

Xinke Liu was born in 1989. He received the B.Sc degree in Hebei Medical University in 2014 and M.sc in Capital Medical University in 2014. He received his resident training in Beijing Tiantan Hospital, Capital Medical University. He is currently a resident doctor at Beijing Tiantan Hospital. His major interest includes endovascular surgery robotic system clinical experiment and black blood imaging and hemodynamic study of intracranial aneurysms.

Youxiang Li was born in 1966. In 1990, he received his B.Sc in Tongji Medical University; in 1998, he received M.sc in Capital Medical University. He received his resident and fellow training in Beijing Tiantan Hospital, Capital Medical University. In 2009 he became the chief of Department of Interventional Neuroradiology, Beijing Neurosurgical Institute and Beijing Tiantan Hospital. His current research interests include endovascular surgery robot system design and vessel wall imaging and hemodynamic study of cerebral vascular disease.